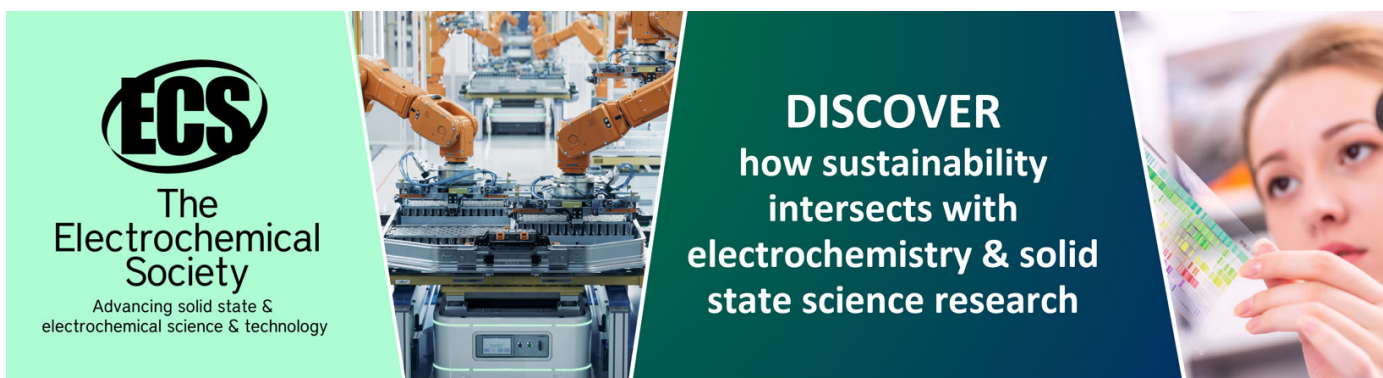# Measurement of electric field development in dielectric barrier discharge in helium

To cite this article: S S Ivković *et al* 2009 *J. Phys. D: Appl. Phys.* **42** 225206

View the article online for updates and enhancements.

Measurement of electric field development in dielectric barrier discharge in helium

S S Ivković[1], **B M Obradović**[1,2], **N Cvetanović**[2,3], **M M Kuraica**[1,2] **and J Purić**[1,2]

[1] Faculty of Physics, University of Belgrade, PO Box 368, 11001 Belgrade, Serbia
[2] Center for Science and Development of Technology, Obilićev Venac 26, 11000 Belgrade, Serbia
[3] Faculty of Transport and Traffic Engineering, University of Belgrade, Vojvode Stepe 305, 11000 Belgrade, Serbia

E-mail: obrat@ff.bg.ac.rs

Abstract
In this paper the diffuse dielectric barrier discharge in helium was investigated using electrical measurements and time–space resolved optical emission spectroscopy. Electric field strength was measured using Stark polarization emission spectroscopy. Investigations were performed at 200 and 800 mbar pressures. It was found that the electric field strength was higher at the higher pressure while cathode fall length was shorter. During the whole discharge development period the length of the cathode fall region decreases. An interesting result is that in the period of current decrease, the maximum of the electric field distribution shifts away from the cathode showing the accumulation of negative charge near the cathode surface.

(Some figures in this article are in colour only in the electronic version)

1. Introduction

Experimental and theoretical studies of dielectric barrier discharges (DBDs), which are convenient plasma sources for the generation of non-thermal plasmas at atmospheric pressure, have received much attention on account of numerous industrial applications [1]. At atmospheric pressure DBD often occurs in the form of a large number of short-lived tiny micro-discharges (filaments), hence that type of discharge is called filamentary. Under special operation conditions in certain gases, a filament-free and transversely uniform mode of the DBD is formed. This diffuse type of discharge is also called homogeneous DBD or atmospheric pressure glow discharge (APGD). The APGD is advantageous compared with the filamentary DBD for applications that require uniform plasma treatment such as the deposition of uniform thin films or surface treatment [2–4].

Although uniform APGDs have been demonstrated in different atmospheres such as helium [5], neon [6] and nitrogen [7], in this paper we focused on helium, in which the APGD was first obtained. APGD in helium is characterized by narrow current pulses ($\sim$1 μs) of large amplitude (tens of milliamperes) and the spatial structure which resembles that of a dc glow discharge at low pressures. The cathode fall, Faraday dark space and positive column develop at the time instant of maximal current [5]. The cathode fall is characterized by a strong electric field, which is responsible for the maintenance of the discharge. Therefore, detailed knowledge of electric field time-dependent distribution is necessary for better understanding of the processes in DBD and their practical applications.

Using the emission spectroscopy technique based on the polarization-dependent Stark splitting and shifting of visible helium lines and their forbidden components, we proposed the method for measurement of the electric field distribution in the cathode region of DBD in helium [8]. In this paper we present time resolved measurements of electric field distribution during evolution of current pulse in the DBD in helium, obtained by this method.

2. Experimental set-up

The experimental set-up is schematically shown in figure 1. The discharge is generated in a parallel plane discharge configuration consisting of two metal electrodes (50×50 mm^2) both covered by a 0.65 mm thick alumina dielectric plates
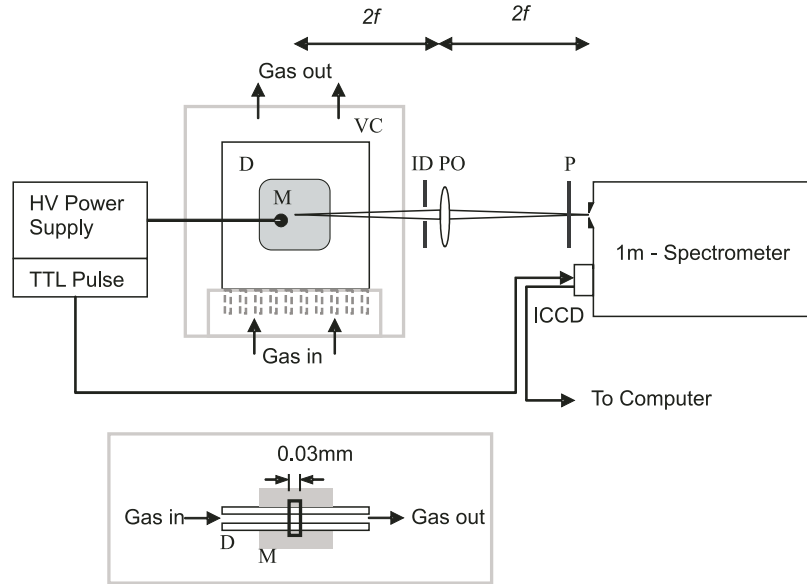
Figure 1. Schematic picture of experimental set-up with a top view of DBD: M—metal electrode, D—dielectric layer, VC—vacuum chamber, ID—iris diaphragm, PO—projection optics, P—polarizer. Bottom picture is a side view of DBD.

$(105 \times 105\,\text{mm}^2;\, \varepsilon_r = 9.4)$. The electrode edges are rounded in order to reduce electric field at sharp edges. The fixed discharge gap of 2 mm is obtained using glass space holders. The discharge cell is placed in a vacuum chamber which is first evacuated down to 10^{-2} mbar, and then filled with helium (purity 99.996%) at 200 or 800 mbar pressure. The gas, with a flow rate of $2\,\text{L}\,\text{min}^{-1}$, is injected into the discharge volume through ten equidistant holes to ensure homogeneous gas flow, see figure 1. The discharge is driven by a home-made pulse voltage power supply. One electrode is kept at ground potential, while on the other a pulse potential with an amplitude of 1.5 kV and a frequency of 5 kHz is applied. The applied voltage U_a is measured via a 1 : 1000 P6015A Tektronics voltage probe; the external total discharge current is monitored using a current probe. The applied voltage and the discharge current are measured by a Tektronics TDS 3032 (300 MHz bandwidth, 2 Gsamples s^{-1}) oscilloscope. The gap voltage U_g is calculated according to the procedure described for unipolar-pulsed DBD in [9]:

$$I_g(t) = \left(1 + \frac{C_g}{C_d}\right) I_t(t) - C_g \frac{\mathrm{d}\,U_a(t)}{\mathrm{d}\,t}, \qquad (1)$$

$$U_g(t) = \frac{C_d}{C_g + C_d} U_a(t) - \frac{1}{C_g + C_d} \int_0^t I_g(\tau)\,\mathrm{d}\tau, \qquad (2)$$

where $U_a(t)$ is the external voltage applied to the DBD cell; $U_g(t)$ the voltage across the discharge gap; $I_t(t)$ the total external current through the DBD cell; $I_p(t)$ the discharge current in the gap. C_d and C_g are equivalent capacitances of the dielectric barrier and the discharge gap, respectively.

The electric field was measured using Stark polarization spectroscopy using wavelength distance between the He I 492.19 nm line (2p ^{1}P^o–4d ^{1}D^o) and its forbidden component (2p ^{1}P^o–4f ^{1}F^o).

For space resolved emission measurements, projection optics is placed at a distance of double focal length $2f$ from the centre of the electrodes and the discharge gap region, displayed in the bottom picture, is imaged 1 : 1 onto the entrance slit of a 1 m spectrometer with 1200 g mm^{-1} diffraction grating, see figure 1. Radiation from the DBD was polarized in the electric field direction (π-polarization) using a plastic polarizer and detected using an ICCD (PI-MAX2, Princeton Instruments) with 256×1024 pixels (pixel dimensions: 26 μm $\times$ 26 μm). ICCD is triggered with a time delayed pulse, generated initially by the power supply. Each recorded image is made of 50 accumulations, each of 50 000 gates per exposure. The gate duration of 100 ns limits the time resolution for investigation of discharge development [10–12]. The gate duration was imposed by the low intensity of the forbidden component of He I 492.19 nm line which is crucial for the electric field measurement. Namely, the electric field was calculated using peak-to-peak wavelength difference between fitted profiles of forbidden and allowed components of He I 492.19 nm spectral line; consequently, the results are very sensitive to the exact position of the forbidden line maximum. With an entrance slit of 30 μm instrumental pseudo-Voigt profile (sum of Gauss and Lorentz profiles) width was 0.028 nm.

3. Results and discussion

One entire period of typical applied voltage signal (voltage applied to the electrodes) is presented in figure 2(*a*) while figures 2(*b*) and (*c*) present the external total current density j_t, external applied U_a and internal gap U_g voltages of glow mode DBD in a 2 mm discharge cell for 200 and 800 mbar pressures. The external applied voltage was pulsed, with voltage drops during the current pulses. These voltage drops originate from the limitations of the power supply. The breakdown voltage was evidently different for different pressures with the same applied voltage. As seen from the figure, negative current pulse is higher and lasts shorter in the discharge at the lower pressure.
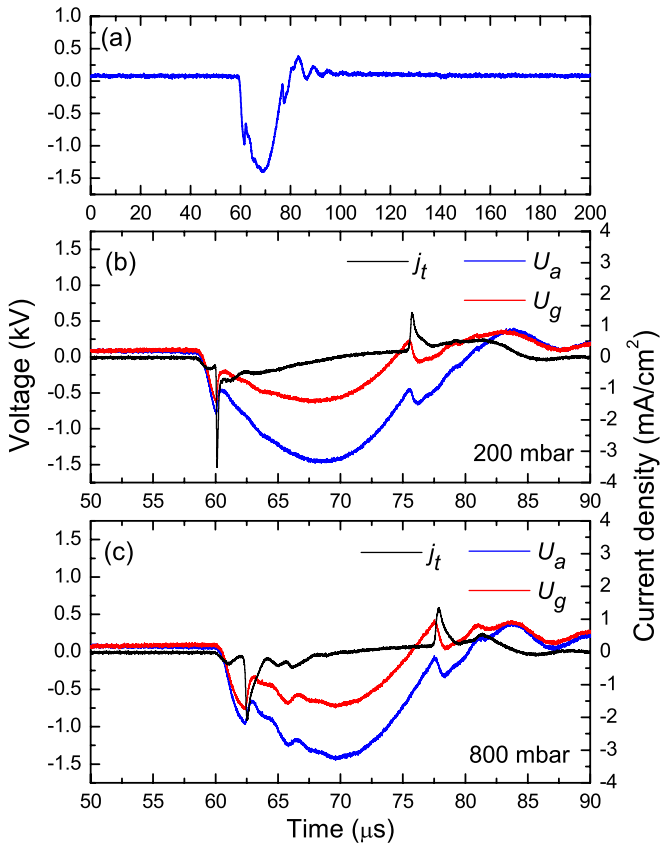
2

Figure 2. (*a*) Example of applied voltage signal of DBD in helium. The external current density, j_t, applied voltage, U_a, and gap voltage, U_g, oscillograms for (*b*) 200 mbar and (*c*) 800 mbar pressures.

Spectroscopy measurements were performed during the negative current signal. Figures 3(*a*) and (*b*) present the ICCD images of He I 492.19 nm line and its forbidden component, recorded at 200 and 800 mbar pressures. It was noted by Navrátil *et al* [13] that helium in DBD is excited by electron impact during the current pulse. This implies that by monitoring the evolution of helium lines we can observe the development of spatial structure of the discharge during the breakdown. This kind of development is characteristic for the Townsend breakdown mechanism. All images are presented with maximal contrast to show, qualitatively, the development of the discharge. The line was recorded in nine successive 100 ns time intervals each with 100 ns exposure marked on current signals shown in figure 4. The line first occurs near the anode and then its intensity increases towards the cathode. The maximum of the line intensity was observed in a time interval denoted as 4 in figure 3(*a*), which is ∼(300 ± 50) ns after the discharge is ignited. A similar development of the same helium line is observed in 800 mbar discharge as shown in figure 3(*b*). The allowed and forbidden helium lines are marked in figure 3(*b*). In figures 5 and 6 distributions of the normalized line intensities in the discharges at 200 and 800 mbar are presented. Each distribution is normalized to its maximum with the intention to simplify the representation of the line development. Some recordings from figure 3 are omitted in figures 5 and 6 because of low line intensity. On analysing the images in figure 3(*a*) and the graphs in figure 5 one can conclude that the line is

ignited near the anode and then propagates to the cathode. In a time interval denoted as 0 ns, which corresponds to the maximal current, the line intensity gets the largest value. The next time interval, denoted as 100 ns, is the beginning of the current decreasing phase, and the maximum of line intensity distribution at the closest position to the cathode surface. Further in the current decreasing phase, the line intensity at the cathode surface decreases and the position of its maximum intensity shifts from the cathode. Although the maximum of the line intensity in the discharge at 800 mbar is observed ∼100 ns later than the line maximum at pressure of 200 mbar, distributions of the line intensity are similar for discharges at both pressures. The shift of the distribution maximum is more evident at lower pressure. It was demonstrated in [12], with high time resolution images (20 ns exposure) of an atmospheric pressure DBD in helium with 5 mm gap, that prior to the strong glow discharge emission near the cathode, first a weak emission near the anode occurs, which is typical for the Townsend discharge. The time for the development of the discharge until it reaches the maximal current value was 460 ns. We also obtained very similar behaviour in our discharge which means that it starts as Townsend and then becomes subnormal, close to the simulation results in [11]. The development of He I 492.19 nm line gives a rough picture of the development of the discharge. To make this picture more precise we measured the electric field evolution during the development of the discharge. By using π-polarized spectra of He I 492.19 nm line, it is possible to obtain the electric field strength reliably at more than 30 points in the cathode sheath region, with a spatial resolution of 40 μm [8]. Electric field influence on He I 492.19 nm line is presented in figure 7, where line profiles are recorded at several distances from the cathode in the DBD in helium at 800 mbar. To simplify the picture, only fitted functions without experimental data are presented for two lines. As seen in the figure, the lines are broad and shifted in the electric field which increases towards the cathode. The line with the lower intensity in the figure is the forbidden component of the helium line and it is more shifted than the allowed line. The origin of line broadening is the overlapping of shifted spectral lines emitted by atoms placed at various positions in the discharge electric field. Namely, when projecting the central region of the discharge onto the entrance slit, the radiation which is detected also includes, besides the radiation from the required region, the radiation from the nearby regions in which the electric field is different.

Using the mentioned spectroscopic method we have measured electric field distributions in several time intervals during the development of the discharge. The results of the measurements in the discharges at 200 mbar and 800 mbar are presented in figures 8 and 9, respectively. For clarity of the figures, error bars are given only for one data point per graph, while they are similar for all other points. Figure 9 has one less graph than figure 8 because of the low intensity of the helium line in that phase of the discharge at 800 mbar. This is due to the low intensity of the forbidden helium line at −100 ns (position 3 in figure 4) in the discharge at 800 mbar, for which the peak wavelength cannot be accurately determined. The negative values of the distance from the cathode are a consequence of light reflection from the alumina layer and
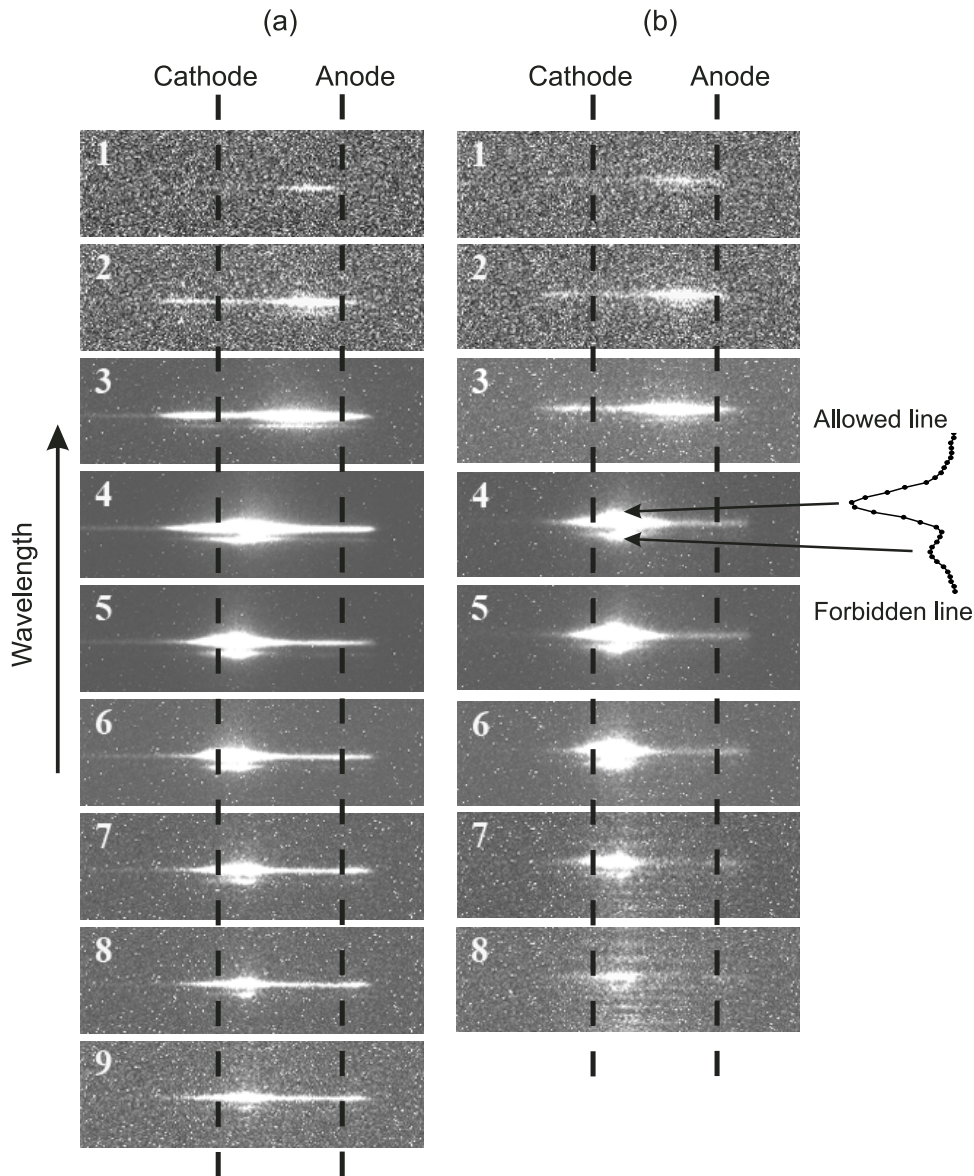
Figure 3. Spatial and temporal evolution of the He I 492.19 nm line in DBD for (*a*) 200 mbar and (*b*) 800 mbar pressures.

have no physical meaning. For those experimental points for which the electric field has evidently linear dependence on the distance from the cathode, we used linear extrapolation as an approximate experimental method for determining the length of the cathode fall region. Namely, the cathode fall length was determined by applying a linear fit at data points and extrapolating linear decrease until the zero field value, see figures 8 and 9.

On analysing figure 8, the following phases of breakdown may be distinguished:

- At the time 100 ns before the maximal current, densities of the charged particles are low, so the external field is not significantly distorted. The cathode fall region is not yet shorter than the length of the discharge gap.
- In the next time interval, the electric field continues to grow near the cathode and drops more steeply due to the space charge approaching the cathode, hence decreasing the cathode fall length. This time interval is characterized

by the maximal external discharge current and the maximal electric field at the cathode of ∼8 kV cm^{-1}.

- In the following three time intervals that belong to the falling edge of the current pulse, the cathode fall length continues to decrease as well as the electric field at the cathode surface. Furthermore, the electric field distribution in the vicinity of the cathode changes the sign of its slope and the maximum of the electric field continuously shifts from the cathode.

A similar development of the electric field distributions is observed in the discharge at 800 mbar. As expected, the length of the cathode fall region is shorter in the discharge at the higher pressure. On the other hand, the electric field at the cathode is ∼11 kV cm^{-1}, which is a larger value than in the 200 mbar discharge.

The length of the cathode fall region close to 0.1 cm in the 800 mbar discharge is larger than in the glow mode of DBDs at atmospheric pressure (0.03–0.04 cm) predicted in [5, 10, 14],
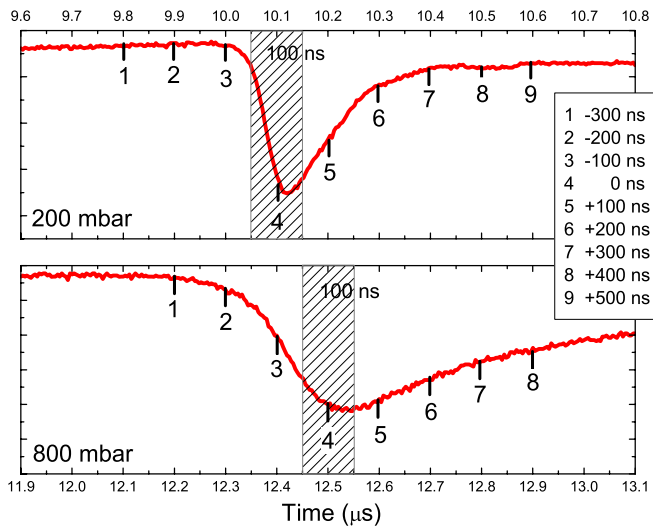
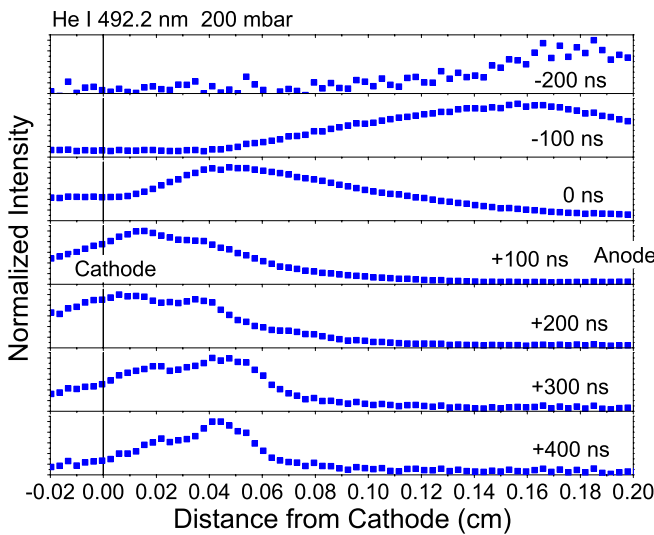**Figure 4.** Current pulses with numbers indicating time instances of image recordings.

Figure 5. Spatial and temporal normalized intensity distributions of He I 492.19 nm in DBD at 200 mbar.

Figure 6. Spatial and temporal normalized intensity distributions of He I 492.19 nm in DBD at 800 mbar.

Figure 7. He I 492.19 nm line recorded at several distances from cathode in DBD in helium at the instance of the maximal current.

Figure 8. Development of the electric field spatial distribution in DBD in helium at 200 mbar.

but it agrees with the so-called Townsend-like mode of the discharge in [10, 15]. Current limitation by the dielectric barrier is crucial in establishing one or the other discharge regime. It was found that the operating point of DBD in atmospheric pressure helium could continuously be adjusted between the glow-like and Townsend-like discharges through an appropriate choice of the dielectric barrier [10]. Limitation of our power supply limited the current in the discharge which caused its operation in the subnormal mode. The decrease in the electric field at the cathode simultaneously with the shortening of the cathode fall length that we observed in the decreasing current phase is predicted in [11]. It is opposite to the expectation that in the decreasing current phase the cathode fall region increases [5].

Our DBD has a length of the cathode fall region similar to the Townsend-like or subnormal-like discharge [10]. These discharge types have a low electric field in the positive column compared with glow-like DBDs [5, 10, 14]. That means that
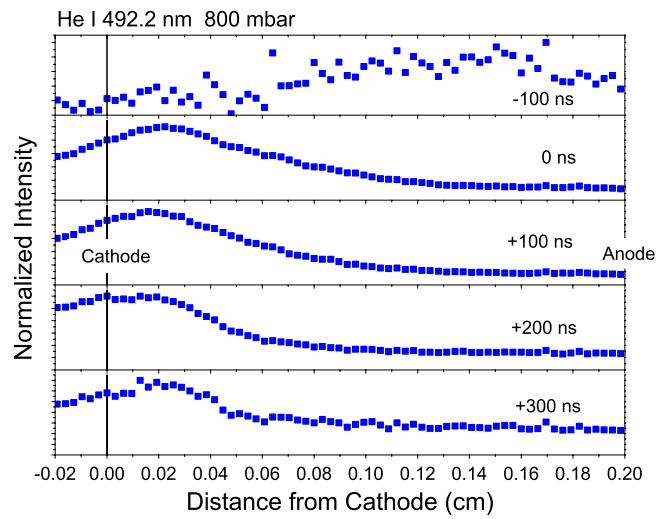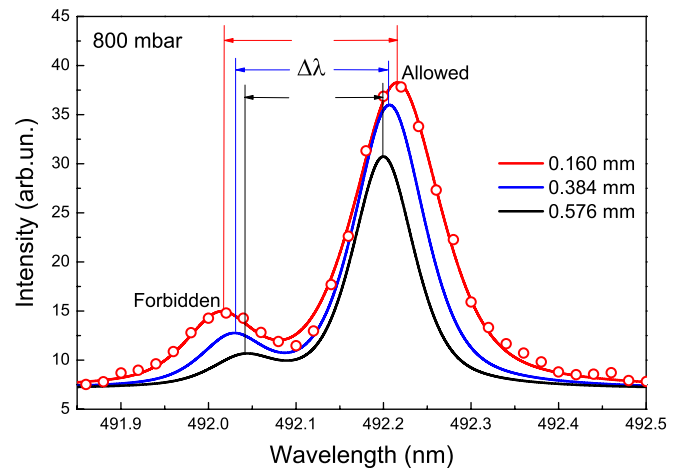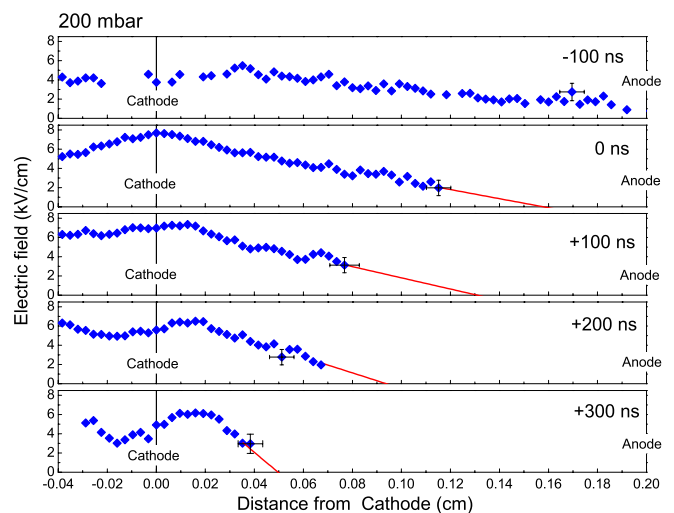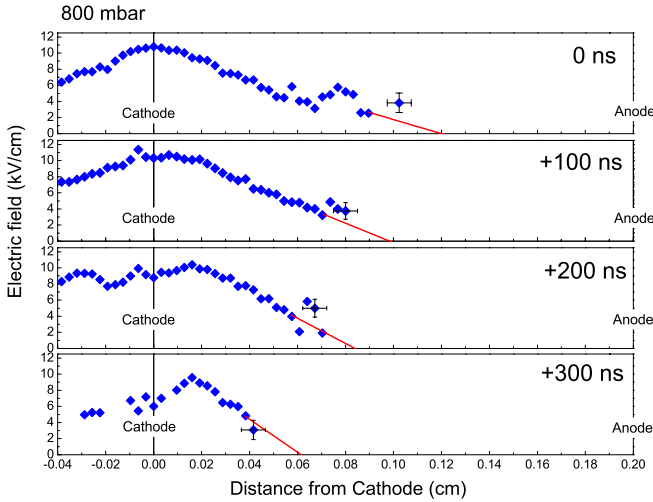
Figure 9. Development of the electric field spatial distribution in DBD in helium at 800 mbar.
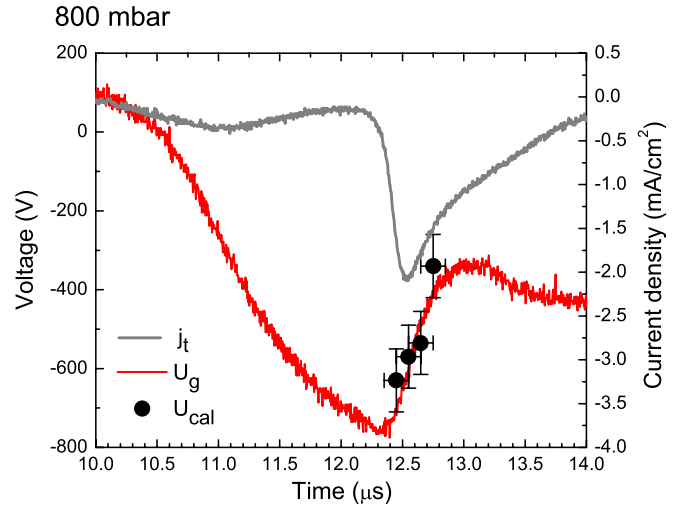

Figure 10. Comparison of calculated cathode fall voltage U_{cal} and measured gap voltage U_g in the DBD at 200 mbar pressure.
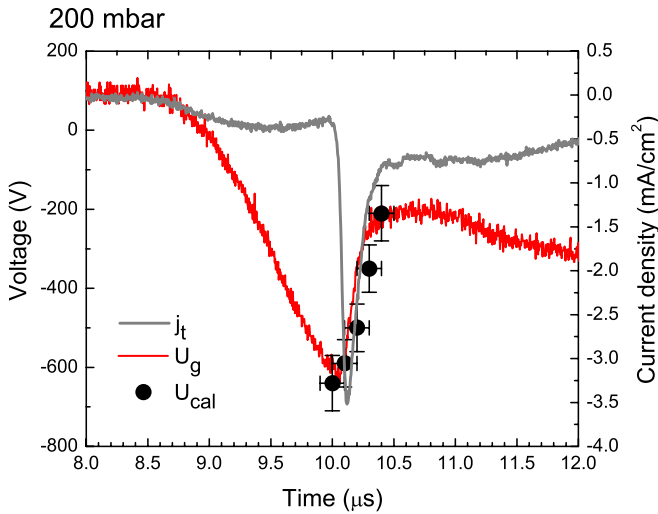

Figure 11. Comparison of calculated cathode fall voltage U_{cal} and measured gap voltage U_g in the DBD at 800 mbar pressure.
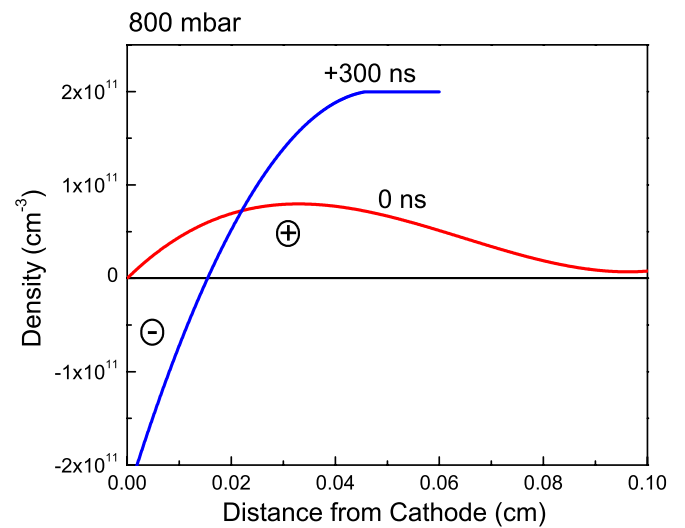

Figure 12. Net space charge density profiles in the cathode region of DBD at 800 mbar during the maximal current, denoted as 0 ns and +300 ns.

almost the entire voltage drop in the discharge belongs to the cathode fall potential drop. To verify our experimental results for the electric field strength, the gap voltage U_g is compared with the cathode fall voltage which is calculated using $U_{cal} = \int_0^L E \, dx$, where L is length of the cathode fall. The calculated cathode fall voltage and gap voltage U_g are presented in figures 10 and 11. Experimental errors of time are estimated taking into account the time jitter during the repetitive line recordings while errors of calculated voltage are determined using the errors presented in figures 8 and 9. A quite good agreement between U_g and U_{cal} convinced us that the electric field measurements in figures 8 and 9 are correct.

An unexpected result that we obtained is the sign change of the slope of the electric field in the vicinity of the cathode. One must take into account that development of the discharge is not uniform in the radial direction of the DBD [16, 17], so the measured electric field has an averaged value of different phases in the discharge evolution. Taking into account experimental [16, 17] and theoretical

[18] investigations of radial development of DBD and our experimental set-up, we estimated that the non-uniformity of our DBD has no significant influence on the measured electric field distributions. The volume where these edge effects are present is too small for the radiation from these regions to significantly influence our measurements.

According to the profiles of the electric field distributions, in the decreasing current phase the overall electric field is reduced, and near the cathode the rising slope of the field is created implying a negative charge build-up.

Finally in figure 12 we present the results of plasma density in two time intervals calculated using the corresponding electric field distribution using the Poisson equation. It can be clearly seen that at low voltages, when the discharge is in the extinguishing phase, a layer of electrons forms near the cathode. Namely, in this period the voltage is reduced and therefore the extraction of the electrons formed by secondary emission is reduced causing a build-up of negative space charge

near the cathode. This negative space charge corresponds to the rising slope of the electric field in figures 8 and 9. Such shapes of electric field and charge density distributions may be found in the literature concerning cathode fall of a low pressure glow discharge [19, 20].

4. Conclusion

Diffuse DBD in helium was investigated using electrical measurements and time–space resolved optical emission spectroscopy. Using the emission spectroscopy technique based on the polarization-dependent Stark splitting and shifting of He I 492.19 nm line and its forbidden component, we measured the electric field distribution in the cathode region of DBD in helium during the evolution of the discharge. For comparison of lengths of the cathode fall regions we used DBD at 200 and 800 mbar pressures. Current density and intensity of the helium line have larger values in the DBD at the lower pressure, whereas the electric field at the cathode is larger at the higher pressure. As expected the electric field strength is shorter at the higher pressure. During the development of the discharge, the length of the cathode fall region decreases at all times and even in the falling phase of the discharge current. In the period of current decrease, the electric field at the cathode decreases, whereas the maximum of the electric field distribution moves from the cathode showing the accumulation of negative charge near the cathode surface.

Acknowledgment

References

[1] Kogelschatz U 2003 Dielectric-barrier discharges: their history, discharge physics and industrial applications *Plasma Chem. Plasma Process.* **23** 1–46

[2] Trunec D, Navrátil Z, St'ahel P, Zajíčková L, Buršíková V and Čech J 2004 Deposition of thin organosilicon polymer films in atmospheric pressure glow discharge *J. Phys. D: Appl. Phys.* **37** 2112–20

[3] Šíra M, Trunec D, St'ahel P, Buršíková V, Navrátil Z and Buršíkov J 2005 Surface modification of polyethylene and polypropylene in atmospheric pressure glow discharge *J. Phys. D: Appl. Phys.* **38** 621–7

[4] Šíra M, Trunec D, St'ahel P, Buršíková V and Navrátil Z 2008 Surface modification of polycarbonate in homogeneous atmospheric pressure discharge *J. Phys. D: Appl. Phys.* **41** 015205

[5] Massines F, Rabehi A, Décomps P, Ben Gadri R, Séguer P and Mayoux C 1998 Experimental and theoretical study of a glow discharge at atmospheric pressure controlled by dielectric barrier *J. Appl. Phys.* **83** 2950–7

[6] Trunec D, Brablec A and Buchta J 2001 Atmospheric pressure glow discharge in neon *J. Phys. D: Appl. Phys.* **34** 1697–705

[7] Gherardi N, Gouda G, Gat E, Ricard A and Massines F 2000 Transition from glow silent discharge to micro-discharges in nitrogen gas *Plasma Sources Sci. Technol.* **9** 340–5

[8] Obradović B M, Ivković S S and Kuraica M M 2008 Spectroscopic measurement of electric field in dielectric barrier discharge in helium *Appl. Phys. Lett.* **92** 191501

[9] Liu S and Neiger M 2003 Electrical modelling of homogeneous dielectric barrier discharges under an arbitrary excitation voltage *J. Phys. D: Appl. Phys.* **36** 3144–50

[10] Mangolini L, Anderson C, Heberlein J and Kortshagen U 2004 Effects of current limitation through the dielectric in atmospheric pressure glows in helium *J. Phys. D: Appl. Phys.* **37** 1021–30

[11] Martens T, Brok W J M, van Dijk J and Bogaerts A 2009 On the regime transitions during the formation of an atmospheric pressure dielectric barrier glow discharge *J. Phys. D: Appl. Phys.* **42** 122002

[12] Luo H, Liang Z, Lv B, Wang X, Guan Z and Wang L 2007 Observation of the transition from a Townsend discharge to a glow discharge in helium at atmospheric pressure *Appl. Phys. Lett.* **91** 221504

[13] Navrátil Z, Brandenburg R, Trunec D, Brablec A, St'ahel P, Wagner H-E and Kopecký Z 2006 Comparative study of dielectric barrier discharges in neon and helium *Plasma Sources Sci. Technol.* **15** 8–17

[14] Golubovskii Y B, Maiorov V A and Behnke J 2003 Modeling of the homogeneous barrier discharge in helium at atmospheric pressure *J. Phys. D: Appl. Phys.* **36** 39–49

[15] Wang Y and Wang D 2006 The role of metastable atoms in a homogeneous atmospheric pressure barrier discharge in helium *Plasma Sci. Technol.* **8** 539–43

[16] Luo H, Liang Z, Lv B, Wang X, Guan Z and Wang L 2007 Radial evolution of dielectric barrier glowlike discharge in helium at atmospheric pressure *Appl. Phys. Lett.* **91** 231504

[17] Mangolini L, Orlov K, Kortshagen U, Heberlein J and Kogelschatz U 2002 Radial structure of a low-frequency atmospheric-pressure glow discharge in helium *Appl. Phys. Lett.* **80** 1722

[18] Zhang P and Kortshagen U 2006 Two-dimensional numerical study of atmospheric pressure glows in helium with impurities *J. Phys. D: Appl. Phys.* **39** 153–63

[19] Brown S C 1959 *Basic Data of Plasma Physics* (New York: MIT and Wiley)

[20] Lieberman M A and Lichtenberg A J 2005 *Principles of Plasma Discharges and Materials Processing* 2nd edn (Hoboken: Wiley)